General Expressions for the Magnetic Flux Density Produced by Axially Magnetized Toroidal Permanent Magnets

Elio A. Périgo[1], Rubens N. Faria[1], and Cláudio C. Motta[2]

[1]Nuclear and Energy Research Institute, IPEN-CNEN/SP, São Paulo 05508-000, Brazil
[2]Brazilian Navy Technology Center, CTMSP, São Paulo 05508-900, Brazil

This paper presents analytical-integral expressions which evaluate the magnetic flux density radial and axial components' on- and off-axis of axially magnetized toroidal permanent magnets. The pieces, when used in magnetic electron beam focusing structures called periodic-permanent magnets (PPMs), can be employed in microwave vacuum electronics devices. These expressions can be adapted to computational algorithms, especially those developed based on mathematical commercial codes, aiding the investigation of the effect of magnetic fields on electron beam dynamics. Comparisons between analytical-integral expressions and theoretical and experimental data are also presented and discussed.

***Index Terms*—Magnetic electron beam focusing system, magnetostatics, off-axis magnetic flux density, periodic-permanent magnet, traveling-wave tubes.**

I. Introduction

A MAGNETIC electron beam focusing system is an essential constituent of power microwave devices, such as klystron amplifiers and traveling-wave tubes (TWTs), which avoids the electron stream spreading due to space-charge forces ensuring suitable electron beam propagation, with diameter approximately constant, through the microwave device drift tube. Thus, the beam constitutes an adequate material medium to be able to convert its own kinetic energy into electromagnetic radio-frequency (RF) power. Magnetic focusing systems can be composed of solenoids, permanent magnets, or both. Details of possible systems and design examples can be found in [1] and [2].

A periodic-permanent magnet (PPM) is a focusing structure which consists of a set of side-by-side toroidal magnets where adjacent pieces repel each other. A schematic drawing is presented in Fig. 1. Each permanent magnet, and consequently the PPM, yields a spatial distribution of the magnetic flux lines which completely fills its interior, as illustrated in Fig. 2. The inner radius of the magnets is several times larger than the beam radius and a ratio above five is not rare. So, when the electron beam propagates along the PPM axis with a magnetic flux density given by $B_\rho(\rho,z)\hat{a}_\rho + B_z(\rho,z)\hat{a}_z$ (the field being considered, by assumption, axially symmetric, i.e., $B_\phi = 0$), the nonrelativistic dynamics of one electron is a solution of

$$\frac{d\vec{v}(\vec{r},t)}{dt} = -\eta\{\vec{E}_{\rm sc}(\vec{r},t) + \vec{v}(\vec{r},t)\times[B_\rho(\rho,z)\hat{a}_\rho + B_z(\rho,z)\hat{a}_z]\} \tag{1}$$

where η is the electron charge to mass ratio, $\vec{E}_{\rm sc}$ is the electric field originated from the space-charge effect, $\vec{v}(\vec{r},t)$ is the electron velocity, B_ρ and B_z denote the radial and the axial components of the magnetic flux density, respectively, and $\hat{a}_\rho$ and $\hat{a}_z$ are the unit vectors. An analysis of (1) shows the relevance of determining analytical expressions that describe both the magnetic axial and radial flux density components, even off-axis ones, which are not frequent in the literature.

Digital Object Identifier 10.1109/TMAG.2007.904708

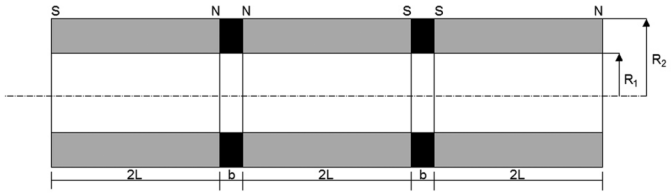

Fig. 1. Schematic drawing of a periodic-permanent magnet (PPM) with axially magnetized toroidal magnets having an inner radius of R_1, outer radius R_2, and thickness $2L$ with space between adjacent magnets b. The polarity of each surface is also presented.

The most common presentation of this kind of result involves Taylor expansions

$$B_\rho(\rho,z) = -\frac{\rho}{2}B_0^{(1)} + \frac{\rho^3}{4\cdot 2^2}B_0^{(3)} - \frac{\rho^5}{6\cdot 2^2\cdot 4^2}B_0^{(5)} + \cdots \tag{2}$$

$$B_z(\rho,z) = B_0 - \frac{\rho^2}{2^2}B_0^{(2)} + \frac{\rho^4}{2^2\cdot 4^2}B_0^{(4)} + \cdots \tag{3}$$

where $B_0 = B_z(\rho = 0, z)$, the axial component, and the superscript number inside the brackets indicative derivatives with respect to axial distance z [4]. An alternative numerical solution was reported recently [5] where the radial and axial magnetic flux densities of a toroidal permanent magnet were obtained from a summation of a term-by-term integration of the scalar magnetic potential

$$\psi(\rho,z) = \frac{M}{\pi}\int_{R_1}^{R_2}\frac{\rho' d\rho'}{[(\rho+\rho')^2 + (z-L)^2]^{(1/2)}}\mathrm{K}(\kappa) \tag{4a}$$

with

$$\kappa = \left[\frac{4\rho\rho'}{(\rho-\rho')^2 + (z-L)^2}\right]^{\frac{1}{2}} \tag{4b}$$

where M is the magnetization, ρ and z are the radial and the axial coordinates where the field is evaluated, ρ' is the integration variable, and $\mathrm{K}(\kappa)$ is the complete elliptic integral of first order. In (4a), only one surface which the unit vector is parallel to the z axis (see the gray portion in Fig. 3) is being considered, so that the term $(z-L)$ must be replaced by $(z+L)$ in order to take into account the whole sample. The calculation of magnetic

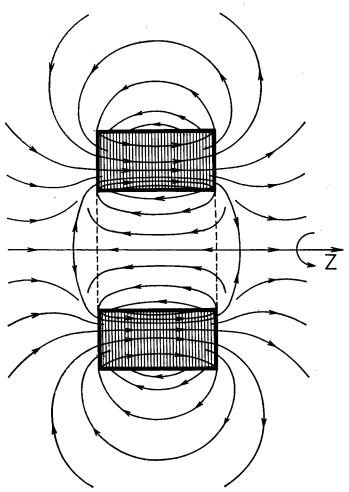

Fig. 2. Magnetic flux density lines of an axially magnetized toroidal permanent magnet [3].

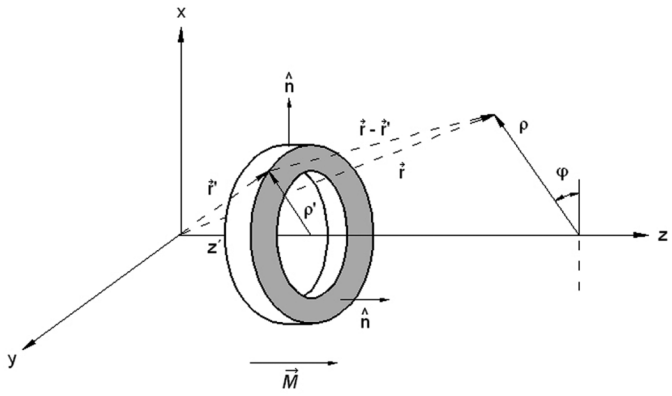

Fig. 3. Geometry used to determine the magnetic flux density for axially magnetized toroidal permanent magnets.

fields produced by permanent magnets with distinct shapes and assemblies using magnetic scalar potential can also be found in literature [6], [7].

The goal of this work is to present a set of analytical-integral expressions that allow the magnetic field profile of toroidal permanent magnets to be determined rapidly, and since no ferromagnetic pieces exist between the magnets, the PPM field profile can be obtained using the superposition principle. As input, it is necessary to know the inner radius R_1, the outer radius R_2, the thickness $2\,L$, and the magnetization M (which can be substituted by the remanence B_r) of each magnet. However, the intrinsic coercivity $\mu_{0i}H_c$ must be larger than B_r in order to avoid the demagnetizing effect.

The paper is organized as follows. Section II describes the simulations and the experimental setup. Section III presents and discusses the development of the analytical-integral expressions, the special case for the axial magnetic flux density on-axis component ($\rho = 0$), and comparisons of the field profile obtained by this method against other techniques and experimental data for a permanent magnet and a theoretical PPM stack. Section IV summarizes the work.

TABLE I
PHYSICAL AND MAGNETIC PROPERTIES OF THE TOROIDAL PERMANENT MAGNETS WITH INNER RADIUS R_1, OUTER RADIUS R_2, THICKNESS $2L$, REMANENCE B_r, AND INTRINSIC COERCIVITY $\mu_{0i}H_c$ EMPLOYED IN THIS WORK

Material	R_1 (mm) (± 2%)	R_2 (mm) (± 2%)	2L (mm) (± 2%)	B_r (mT) (± 2%)	$\mu_{0i}H_c$ (mT)
Ferrite	8.9	19.9	6.0	250	$< B_r$
NdFeB	9.5	17.0	10.0	1300	$> B_r$

TABLE II
PHYSICAL AND MAGNETIC PROPERTIES OF THE THEORETICAL PPM FOCUSING STRUCTURE EVALUATED. PERMANENT MAGNETS PRESENT INNER RADIUS R_1, OUTER RADIUS R_2, THICKNESS $2\,L$, REMANENCE B_r, AND INTRINSIC COERCIVITY $\mu_{0i}H_c$, AND ARE SEPARATED BY b

Material	NdFeB
Number of permanent magnets	20
R_1 (mm)	9.5
R_2 (mm)	17.0
2L (mm)	10.0
B_r (mT)	1300
$\mu_{0i}H_c$ (mT)	$> B_r$
b (mm)	2.0

II. EXPERIMENTAL SETUP AND SIMULATIONS

Commercial ferrite and NdFeB axially magnetized toroidal permanent magnets were used to assemble and measure the $B_z(\rho, z)$ profile. The experimental data were taken using an 8-mm diameter Hall sensor coupled to a 2-D precision table with 1 mm of spatial resolution. Table I presents the physical and magnetic features of the magnets. In this way, the experimental results could be compared with those obtained from Taylor expansion and proposed analytical-integral expression. Comparisons were also made between proposed analytical-integral expressions and the Taylor expansion for a hypothetical PPM stack with 20 magnets using a commercial mathematical software program. Table II shows the characteristics of the focusing system considered in this work.

III. RESULTS AND DISCUSSION

A. Proposed Method

From the potential theory, the magnetic flux density produced by an axially magnetized toroidal permanent magnet, externally to the material, can be found using the magnetic scalar potential $\psi(\vec{r})$, where $\vec{B}(\vec{r}) = -\nabla\psi(\vec{r})$, given by [5]

$$\psi(\vec{r}) = \frac{1}{4\pi}\int \frac{M(\vec{r}') \cdot \hat{n}}{|\vec{r} - \vec{r}'|} dS' \tag{5}$$

where M is the magnetization, $\vec{r}$ is the field point, $\vec{r}'$ is the source point, $\hat{n}$ is a normal unit vector to the permanent magnet surface, and $dS' = \rho' d\rho' d\varphi'$. Due to the dot product in (5), only

the upper and lower surfaces of the magnet analyzed here contribute with $\psi(\vec{r})$ (see the gray portion in Fig. 3). Hence

$$\psi_{\sup}(\vec{r}) = \frac{M}{4\pi}\int_{R_1}^{R_2}\int_{0}^{2\pi}\frac{\rho' d\rho' d\varphi'}{|\vec{r}-\vec{r}'|}. \quad (6)$$

The term $|\vec{r}-\vec{r}'|^{-1}$ in (6) can be replaced using an integral transformation in terms of real functions, as presented below [8]

$$\frac{1}{|\vec{r}-\vec{r}'|} = \frac{4}{\pi}\int_0^\infty dk\cos[k(z-z')]\left\{\frac{1}{2}I_0(k\rho_<)K_0(k\rho_>) + \sum_{m=1}^{\infty}\cos[m(\varphi-\varphi')]I_m(k\rho_<)K_m(k\rho_>)\right\} \quad (7)$$

where $\rho_<(\rho_>)$ is smaller (larger) than ρ' and ρ. Considering $\varphi = 0$

$$\psi_{\sup}(\vec{r}) = \frac{M}{\pi^2}\int_0^\infty dk\cos[k(z-L)]\int_{R_1}^{R_2}\int_0^{2\pi}\left\{\frac{1}{2}I_0(k\rho_<)K_0(k\rho_>) + \sum_{m=1}^{\infty}\cos(m\varphi')I_m(k\rho_<)K_m(k\rho_>)\right\}\rho' d\rho' d\varphi' \quad (8)$$

where I_m and K_m are the modified Bessel functions of order m of the first and second type, respectively. The first integral evaluated was the azimuthal one in (8), carried out using the cosine orthogonality properties. Therefore

$$\psi_{\sup}(\vec{r}) = \frac{M}{\pi}\int_0^\infty dk\cos[k(z-L)]\int_{R_1}^{R_2} I_0(k\rho_<)K_0(k\rho_>)\rho' d\rho'. \quad (9)$$

Taking into account the integration in the radial variable in (9), two situations must be considered: a) if $\rho_< = \rho'$, then

$$\int_{R_1}^{R_2} I_0(k\rho')K_0(k\rho)\rho' d\rho' = K_0(k\rho)\int_{R_1}^{R_2} I_0(k\rho')\rho' d\rho' \quad (10)$$

and, using a relation given in [9], (10) becomes

$$\int_{R_1}^{R_2} I_0(k\rho')K_0(k\rho)\rho' d\rho' = K_0(k\rho)\frac{1}{k}[(R_2)I_1(kR_2) - (R_1)I_1(kR_1)]; \quad (11)$$

b) if $\rho_< = \rho$, then

$$\int_{R_1}^{R_2} I_0(k\rho)K_0(k\rho')\rho' d\rho' = I_0(k\rho)\int_{R_1}^{R_2} K_0(k\rho')\rho' d\rho' \quad (12)$$

and, using another relation given in [9], (12) becomes

$$\int_{R_1}^{R_2} I_0(k\rho)K_0(k\rho')\rho' d\rho' = -I_0(k\rho)\frac{1}{k}[(R_2)K_1(kR_2) - (R_1)K_1(kR_1)]. \quad (13)$$

Grouping (12) and (13) in (9), one has

$$\psi_{\sup}(\vec{r}) = -\frac{M}{\pi}\int_0^\infty dk\cos[k(z-L)]I_0(k\rho)\frac{1}{k} \times[(R_2)K_1(kR_2) - (R_1)K_1(kR_1)] \quad (14)$$

for $\rho < R_1$, and

$$\psi_{\sup}(\vec{r}) = \frac{M}{\pi}\int_0^\infty dk\cos[k(z-L)]K_0(k\rho)\frac{1}{k} \times[(R_2)I_1(kR_2) - (R_1)I_1(kR_1)] \quad (15)$$

for $\rho > R_2$.

The radial component of the magnetic flux density for $\rho < R_1$ will be given by

$$B_\rho(\vec{r}) = -\frac{M}{\pi}\int_0^\infty dk\cos[k(z-L)]I_1(k\rho) \times[(R_2)K_1(kR_2) - (R_1)K_1(kR_1)] \quad (16)$$

and, for $\rho > R_2$, by

$$B_\rho(\vec{r}) = \frac{M}{\pi}\int_0^\infty dk\cos[k(z-L)]K_1(k\rho) \times[(R_2)I_1(kR_2) - (R_1)I_1(kR_1)]. \quad (17)$$

The axial magnetic flux density component for $\rho < R_1$ is written by

$$B_z(\vec{r}) = \frac{M}{\pi}\int_0^\infty dk\sin[k(z-L)]I_0(k\rho) \times[(R_2)K_1(kR_2) - (R_1)K_1(kR_1)] \quad (18)$$

and, for $\rho > R_2$, by

$$B_z(\vec{r}) = -\frac{M}{\pi}\int_0^\infty dk\sin[k(z-L)]K_0(k\rho) \times[(R_2)I_1(kR_2) - (R_1)I_1(kR_1)]. \quad (19)$$

The expressions (16)–(19) describe the B_ρ and B_z of just one magnetically charged surface of a toroidal permanent magnet with inner radius R_1, outer radius R_2, thickness $2\,L$, and magnetization M (or remanence B_r). In order to obtain the field profile of the whole sample, the term $(z-L)$ must also be considered. Furthermore, it should be noted that expressions (16)–(19) are exact solutions of the field equations and no additional terms are

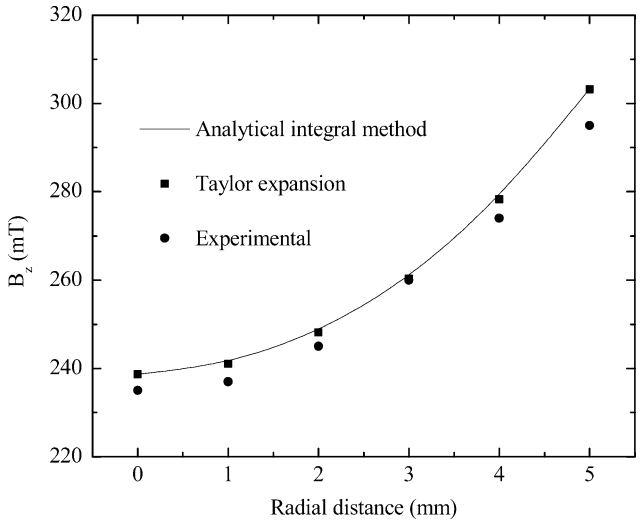

Fig. 4. Comparison of the axial magnetic flux density profile (experimental and obtained from analytical-integral expression and Taylor expansion) of a toroidal permanent magnet for $z = 0$ along ρ, for $\rho < R_1$, with $R_1 = 9.5$ mm, $R_2 = 17.0$ mm, $2L = 10.0$ mm, and $B_r = 1.30$ T.

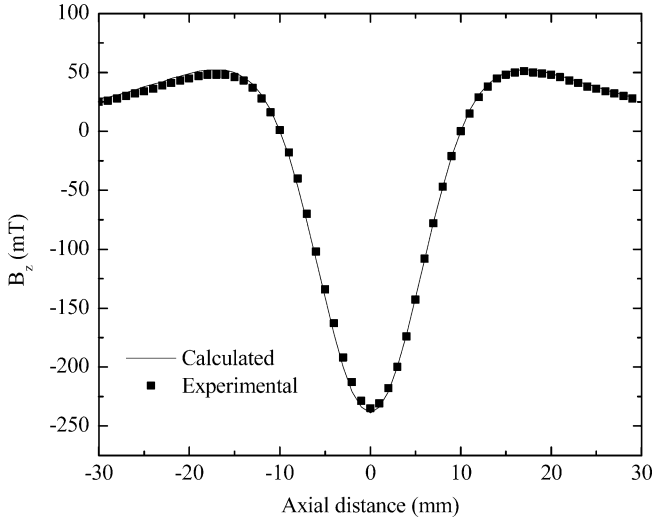

Fig. 5. Comparison of theoretical and experimental axial magnetic flux density profiles of a toroidal permanent magnet for $\rho = 0$ with $R_1 = 9.5$ mm, $R_2 = 17.0$ mm, $2L = 10.0$ mm, and $B_r = 1.30$ T.

necessary to compute the radial and axial magnetic flux densities, unlike the case of the Taylor expansion or even of (4a).

It is relevant to verify if these expressions satisfy the $\nabla \cdot \vec{B} = 0$ condition. For any point inside the toroidal magnet ($\rho < R_1$), the axial and radial magnetic flux density components are, respectively

$$\frac{1}{\rho}\frac{\partial}{\partial\rho}\rho B_\rho(\rho,z) = -\frac{M}{\pi}\int_0^\infty dk\cos[k(z-L)]kI_0(k\rho) \times[(R_2)K_1(kR_2)-(R_1)K_1(kR_1)] \quad (20)$$

$$\frac{\partial}{\partial z}B_z(\rho,z) = \frac{M}{\pi}\int_0^\infty dk\cos[k(z-L)]kI_0(k\rho) \times[(R_2)K_1(kR_2)-(R_1)K_1(kR_1)] \quad (21)$$

and, analyzing (20) and (21), it is verified that $\nabla \cdot \vec{B} = (1/\rho)(\partial/\partial\rho)(\rho B_\rho)+(\partial/\partial z)B_z = 0$, as expected. For $\rho > R_2$, the expressions for the fields taking into account their derivates are

$$\frac{1}{\rho}\frac{\partial}{\partial\rho}\rho B_\rho(\rho,z) = \frac{M}{\pi}\int_0^\infty dk\cos[k(z-L)]kK_0(k\rho) \times[(R_2)I_1(kR_2)-(R_1)I_1(kR_1)] \quad (22)$$

$$\frac{\partial}{\partial z}B_z(\rho,z) = -\frac{M}{\pi}\int_0^\infty dk\cos[k(z-L)]kK_0(k\rho) \times[(R_2)I_1(kR_2)-(R_1)I_1(kR_1)] \quad (23)$$

so that, using (22) and (23), it is also verified that $\nabla \cdot \vec{B} = (1/\rho)(\partial/\partial\rho)(\rho B_\rho) + (\partial/\partial z)B_z = 0$.

B. On-Axis Magnetic Flux Density Component: A Special Case

A special case of the analytical-integral expressions presented here involves the determination of the axial magnetic flux density component on-axis of the toroidal magnet, that is, $\rho = 0$. In this case, (18) reduces to

$$B_z(0,z) = -\frac{M}{\pi}\int_0^\infty dk\sin[k(z-L)] \times[(R_2)K_1(kR_2)-(R_1)K_1(kR_1)] \quad (24)$$

since $I_0(0) = 1$. Equation (24) can be solved from the result [10]

$$\int_0^\infty K_1(ka)\sin(kz)dk = \frac{\pi}{2a}\frac{z}{\sqrt{z^2+a^2}} \quad (25)$$

and by replacing (25) for (24)

$$B_z(0,z) = \frac{M}{2}\left[\frac{z-L}{\sqrt{(z-L)^2+R_2^2}} - \frac{z-L}{\sqrt{(z-L)^2+R_1^2}}\right]. \quad (26)$$

Additionally, it is necessary to consider the magnetic flux density from the lower surface of the magnet, which will be given by

$$B_z(0,z) = -\frac{M}{2}\left[\frac{z+L}{\sqrt{(z+L)^2+R_2^2}} - \frac{z+L}{\sqrt{(z+L)^2+R_1^2}}\right] \quad (27)$$

so that, due to the contributions of both (26) and (27), the axial magnetic flux density component for an axially magnetized toroidal permanent magnet is written as

$$B_z(0,z) = \frac{M}{2}\left\{\left[\frac{z+L}{\sqrt{(z+L)^2+R_2^2}} - \frac{z-L}{\sqrt{(z-L)^2+R_2^2}}\right] - \left[\frac{z+L}{\sqrt{(z+L)^2+R_1^2}} - \frac{z-L}{\sqrt{(z-L)^2+R_1^2}}\right]\right\} \quad (28)$$

which is the same expression as that obtained by Peng *et al.* [11]. Using the superposition principle, the axial magnetic flux density component on-axis of a PPM stack without pole pieces with N permanent magnets is

$$B_z(0,z)=\sum_{i=0}^{N}(-1)^i\frac{M}{2}\left\{\begin{array}{l}\left[\frac{z+L+(i\{2L+b\})}{\sqrt{(z+L+\{i[2L+b]\})^2+R_2^2}}-\frac{z-L+(i\{2L+b\})}{\sqrt{(z-L+\{i[2L+b]\})^2+R_2^2}}\right]\\-\left[\frac{z+L+(i\{2L+b\})}{\sqrt{(z+L+\{i[2L+b]\})^2+R_1^2}}-\frac{z-L+(i\{2L+b\})}{\sqrt{(z-L+\{i[2L+b]\})^2+R_1^2}}\right]\end{array}\right\} \tag{29}$$

where b is the distance between adjacent permanent magnets. If just one permanent magnet is analyzed using (29), $N=0$ and (28) is obtained, as expected. However, a more general expression can be found using the analytical-integral method developed here. The axial magnetic flux density for any point inside the magnet, that is, $\rho<R_1$, is given by

$$B_z(0,z)=\sum_{i=0}^{N}(-1)^i\frac{M}{\pi}\left\{\left[\begin{array}{l}\int\sin(k\{z-L+[i(2L+b)]\})I_0(k\rho)(R_2K_1(kR_2)-R_1K_1(kR_1))dk\\-\int\sin(k\{z+L+[i(2L+b)]\})I_0(k\rho)(R_2K_1(kR_2)-R_1K_1(kR_1))dk\end{array}\right]\right\}. \tag{30}$$

Equation (30) makes it possible to design PPM structures with magnets of any inner radius R_1, outer radius R_2, and thickness $2L$. Remanence and spacing between toroids are usually kept constant in order to maintain a $B_z(0,z)$ sinusoidal profile and intensity. No ferromagnetic pieces are considered between the magnets.

C. Theoretical and Experimental Evaluation of Analytical-Integral Expressions

Fig. 4 compares the analytical-integral method, Taylor expansion, and experimental profile plots of the axial magnetic flux density component along ρ for $z=0$, at the center of the NdFeB sample. An increase in the $B_z(\rho,0)$ values can be observed for points closer to the internal surface of the analyzed magnet. The three field profiles are almost coincident from $\rho=0$ to $\rho=5$ mm and the average discrepancy between theoretical and experimental data is about 3%. A possible reason for this difference is the measurement system employed. Since the precision in the radial distance is 1 mm, small variations in the Hall sensor position may cause the deviations observed. An important feature of this analysis is that $\rho=5$ mm refers to a dimension larger than the usual electron beam radius (about 2 mm), so that the analytical-integral method applies successfully to evaluate the influence of a spatial distribution of a magnetic field on electron beam dynamics.

Considering the axis of symmetry of the permanent magnet, Fig. 5 depicts both theoretical (obtained from (30) for $i=0$ and $\rho=0$) and experimental $B_z(0,z)$ profiles, which show an excellent congruence. Discrepancy was kept below 2%.

Fig. 6(a)–(c) compares the experimental data against the three methods presented in this paper (Taylor expansion, integration of the scalar magnetic potential, and analytical-integral solution) for the ferrite sample of the axial magnetic flux density component along the axis of symmetry for $\rho=0$, $\rho=1$ mm, and $\rho=2$ mm. Note the excellent congruence of the proposed

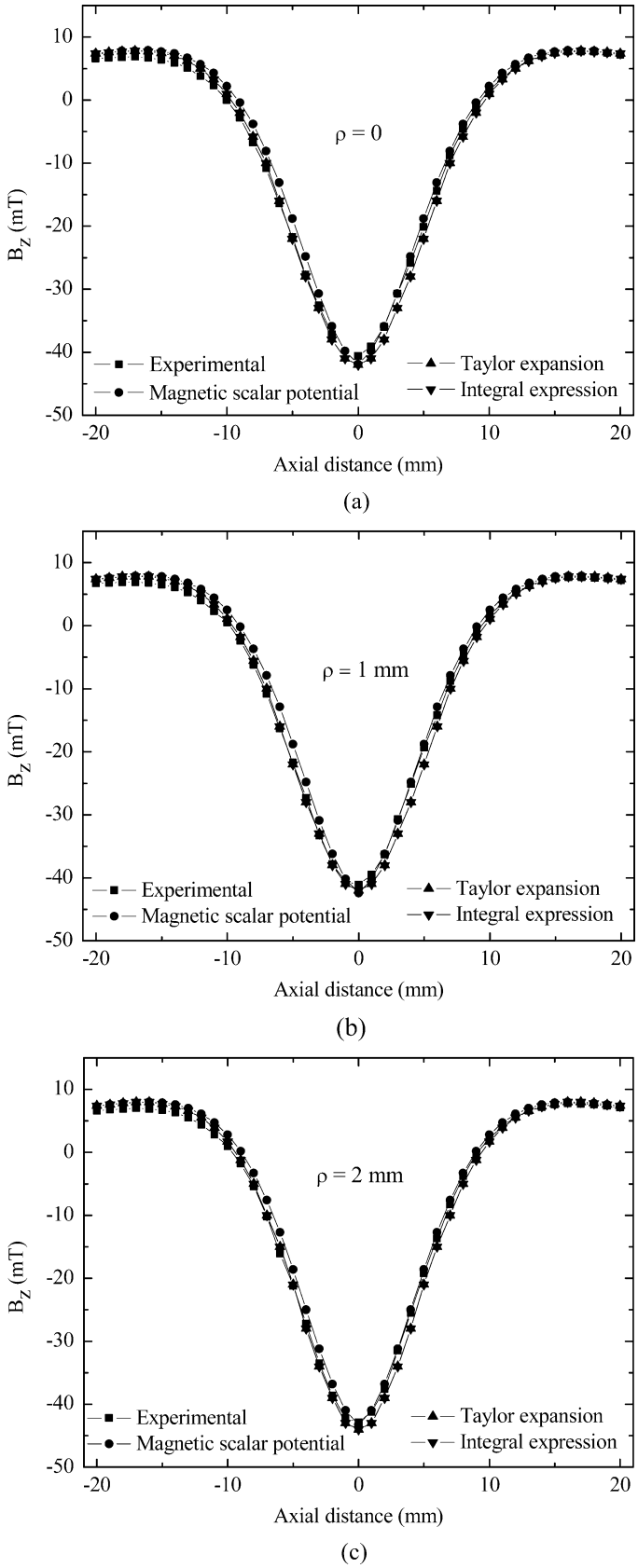

Fig. 6. Comparison of experimental and calculated axial magnetic flux density profiles of a toroidal ferrite magnet for (a) $\rho=0$, (b) $\rho=1$ mm, and (c) $\rho=2$ mm.

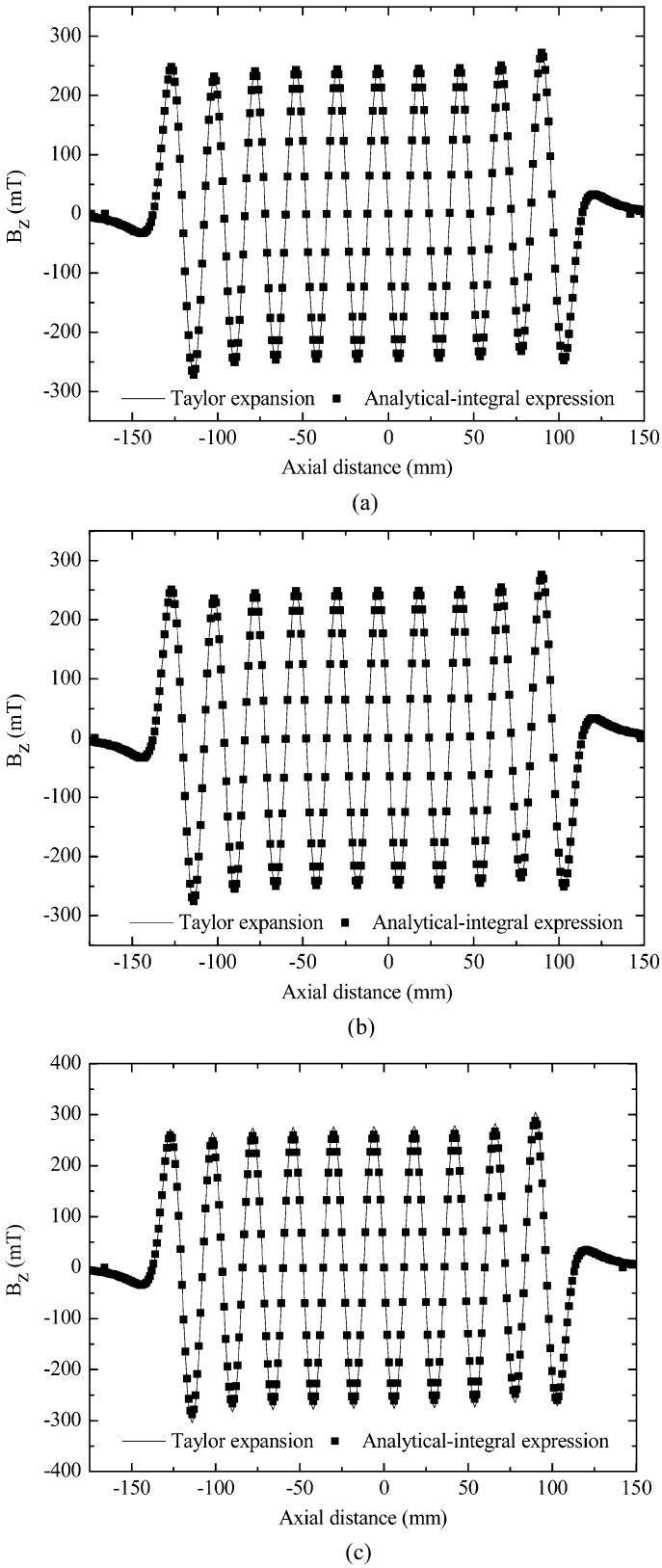

Fig. 7. Axial magnetic flux density component profiles obtained using the Taylor expansion and the analytical-integral expression (30) of the PPM designed for (a) $\rho = 0$, (b) $\rho = 1$ mm, and (c) $\rho = 2$ mm.

solution and the measured values of $B_z(\rho)$, since the disparity remained at around 5% in every situation evaluated.

TABLE III
AXIAL MAGNETIC FLUX DENSITY COMPONENT ALONG z FOR $\rho = 0$, $\rho = 1$ mm, AND $\rho = 2$ mm FOR THE PPM STRUCTURE DESIGNED (VALUES EXPRESSED IN mT)

Peak	ρ = 0		ρ = 1 mm		ρ = 2 mm	
	Taylor	AI	Taylor	AI	Taylor	AI
1	248	248	251	251	272	260
2	-272	-272	-280	-276	-305	-288
3	232	232	240	236	265	248
4	-251	-251	-259	-255	-283	-267
5	241	241	250	245	274	258
6	-246	-246	-254	-250	-279	-263
7	243	243	252	248	276	260
8	-245	-245	-253	-249	-278	-262
9	244	244	252	248	277	261
10	-245	-245	-253	-249	-277	-261
11	245	245	253	249	277	261
12	-244	-244	-252	-248	-277	-261
13	245	245	253	249	278	262
14	-243	-243	-252	-248	-276	-260
15	246	246	254	250	279	263
16	-241	-241	-250	-245	-274	-258
17	251	251	259	255	283	267
18	-232	-232	-240	-236	-265	-248
19	272	272	280	276	305	288
20	-248	-248	-251	251	-272	-260

*AI = Analytical-Integral – expression (30)

Fig. 7(a)–(c) compares the $B_z(0,z)$ profile of a PPM stack with 20 permanent magnets having $\rho = 0$, $\rho = 1$ mm, and $\rho = 2$ mm using the analytical-integral expression proposed [(30) and Taylor expansion]. Sinusoidal field profiles were obtained in each case, as expected. Table III presents the values of the axial magnetic flux density component obtained by both methods for each peak. No discrepancy between the values was found for $\rho = 0$, which corresponds to the special case already discussed. For $\rho = 1$ mm, the analytical-integral method presented values about 2% lower than that obtained with the Taylor expansion. Lastly, for $\rho = 2$ mm, the difference between the methods increased to 6%, possibly due to the number of terms of the Taylor expansion and the limits of the integration used in the analytical-integral expression.

It can also be noted that peaks #2 and #19 presented a higher $B_z(z)$ value than that obtained at the center of the structure in each situation. This is due to the end effect. In a PPM system,

the magnets contribute to the $B_z(\rho, z)$ value at every point and this contribution decreases as the distance between the analyzed point and the magnet increases. At the center of the stack, all the magnets "work" under the same conditions. However, at the ends of the PPM, part of the magnetic field does not exist due to the distance between the region in question and the series of magnets. Thus, B_z is expected to present a higher value.

It is worth pointing out that this PPM analysis is valid, since the intrinsic coercivity of the magnets is larger than their remanence. This is the essential condition for the magnets to remain magnetically stable within the stack, which is achieved for NdFeB and SmCo compounds by controlling the chemical composition of the raw material. For this reason, each magnet can be treated individually and the superposition principle can be applied successfully. The presence of ferromagnetic pole pieces between magnets changes this analysis because their relative permeability differs from unity and a magnetic boundary condition problem should be solved.

IV. Conclusion

Analytical-integral expressions which determine the axial and radial magnetic flux density components of axially magnetized toroidal permanent magnets, either on- or off-axis, were presented. Comparisons between theoretical and experimental field profiles for ferrite and NdFeB samples revealed quite a satisfactory agreement.

The field profile of a PPM was obtained by means of the superposition effect. However, this is valid for magnets with $\mu_{0i}H_c > B_r$. The comparison between the analytical-integral method and the Taylor expansion showed a good agreement. The end effect was also predicted for both methods.

Acknowledgment

The authors wish to thank CTMSP and IPEN-CNEN for providing the facilities required for this investigation. This work was supported in part by the State of São Paulo Research Foundation (FAPESP) under Grant 05/04711-2 and the National Council for Scientific and Technological Development (CNPq) under process number 305812/2005-0.

References

[1] E. A. Périgo, J. J. Barroso, and C. C. Motta, "A hybrid magnetic focusing system for microwave tubes," *IEEE Trans. Plasma Sci.*, vol. 34, no. 5, pp. 1789–1795, Oct. 2006.

[2] S. Liu, "Optimum design on the focusing magnetic field for MMW TWTs," *Int. J. Infrared Millim. Waves*, vol. 22, no. 3, pp. 399–405, Mar. 2001.

[3] E. Durand, *Magnetostatique*. Paris, France: Masson, 1968.

[4] K. R. Spangemberg, *Vacuum Tubes*. New York: McGraw-Hill, 1948.

[5] E. A. Périgo, C. S. Muranaka, and C. C. Motta, "Off-axis magnetic flux density of a PPM focusing system," in *Proc. 7th IEEE Int. Vac. Elect. Conf.*, Monterey, CA, Apr. 2006, pp. 367–368.

[6] H. L. Rakotoarison, J.-P. Yonnet, and B. Delinchant, "Using Coulombian approach for modeling scalar potential and magnetic field of a permanent magnet with radial polarization," *IEEE Trans. Magn.*, vol. 43, no. 4, pp. 1261–1264, Apr. 2007.

[7] Y. Zhilichev, "Calculation of magnetic field of tubular permanent-magnet assemblies in cylindrical bipolar coordinates," *IEEE Trans. Magn.*, vol. 43, no. 7, pp. 3189–3196, Jul. 2007.

[8] J. D. Jackson, *Classical Electrodynamics*, 2nd ed. New York: Wiley, 1975.

[9] E. A. Périgo, "Development of a magnetic focusing system using a periodic permanent magnet stack for power microwave devices," M.S. dissertation, Univ. São Paulo, São Paulo, Brazil, 2005.

[10] I. S. Gradshteyn and I. M. Ryzhik, *Tables of Integrals, Series and Products*. San Diego, CA: Academic, 1994.

[11] Q. L. Peng, S. M. McMurry, and J. M. D. Coey, "Axial magnetic field produced by axially and radially magnetized permanent rings," *J. Magn. Magn. Mater.*, vol. 268, pp. 165–169, 2004.

Manuscript received April 4, 2007; revised July 18, 2007. Corresponding author: E. A. Perigo (e-mail: eaperigo@ieee.org).